Electronic Supplementary Material (ESI) for Materials Advances.
This journal is © The Royal Society of Chemistry 2020

Supporting Information

Influence of Different Bismuth Oxyhalides on Photocatalytic Activity of Graphitic Carbon Nitride: A Comparative Study under Natural Sunlight

Mahender Singh,[#] Ashish Kumar[#] and Venkata Krishnan*

School of Basic Sciences and Advanced Materials Research Center, Indian Institute of Technology Mandi, Kamand, Mandi 175075, Himachal Pradesh, India.

[#]These authors contributed equally to this work.

**Corresponding author. Email:* vkn@iitmandi.ac.in

Sl. No.	Contents	Pg. No.
1	Materials characterization	S-2
2	**Fig. S1** XPS survey spectra of g-C_3N_4, BiOBr and BiOBr/g-C_3N_4 composite.	S-3
3	**Fig. S2** Tauc plots for (a-d) BiOX (X = F, Cl, Br and I) and (e) g-C_3N_4.	S-4
4	**Fig. S3** Time dependent UV-vis absorption spectra of CR dye degradation using (a) BiOF, (b) BiOCl, (c) BiOBr, (d) BiOI, (e) g-C_3N_4 and (f) without any photocatalyst (photolysis).	S-5
5	**Fig. S4** Time dependent UV-vis absorption spectra of CR dye degradation using (a) BiOF/g-C_3N_4, (b) BiOCl/g-C_3N_4, (c) BiOBr/g-C_3N_4 and (d) BiOI/g-C_3N_4 composites.	S-6
6	**Fig. S5** Time dependent UV-vis absorption spectra of CBZ fungicide using BiOBr/g-C_3N_4 composite.	S-7
7	**Table S1** Kinetics parameters for CR dye degradation over different photocatalysts.	S-8
8	**Fig. S5** FTIR spectra of fresh and recovered BiOBr/g-C_3N_4 composite.	S-9

Materials characterization

The crystal structure of the as synthesized materials was examined by powder x-ray diffraction (XRD) using Rigaku SmartLab 9 kW rotating anode diffractometer working in Bragg-Brentano configuration with Ni-filtered Cu K_α irradiation (λ = 0.1542 nm) at 45 kV and 100 mA. The scan was done in the 2θ range from 10° to 90° with scan rate of 2° per minute. The Fourier transform infrared (FTIR) spectroscopic studies were carried out for functional group analysis by utilizing an Agilent K8002AA Carry 660 instrument. The morphological and compositional analysis of the prepared samples were done using the Field-emission scanning electron microscopy (FESEM) on FEI Nova Nano SEM-450 instrument. To make the samples conducting, 5 nm Au layer was sputter-coated over them before the FE-SEM measurements. The elemental mapping and energy dispersive x-ray analysis (EDAX) measurements were also performed using the same instrument in order to investigate the presence and spatial distribution of constituent elements. Transmission electron microscopy (TEM) images were taken by a Tecnai G 20 (FEI) S-twin microscope operating at 200 kV (accelerating voltage). The selected area electron diffraction (SAED) pattern, EDAX and dark field imaging were also carried out by using the same TEM instrument. The x-ray photoelectron spectroscopy (XPS) measurements were performed on a ThermoFisher Scientific NEXSA photoelectron spectrometer with Al K_α (1486.6 eV) dual anode as the source, operating at 12 kV anode voltage and 6.50 mA filament current. The sample preparation was carried out by drop-casting the powder catalyst dispersed in ethanol on the silicon wafer. The XPS data were collected on the dried silicon substrate containing the sample with a pass energy of 50 eV at 9 x 10^{-8} mbar vacuum and the analysis of the obtained data was performed using Avantage software. In order to study the light harvesting capability of the prepared samples, diffuse reflectance spectroscopy (DRS) measurements were performed using a Perkin Elmer UV-visible-NIR Lambda 750 spectrophotometer, wherein polytetrafluoroethylene (PTFE) polymer was taken as the diffuse reflectance standard. The photoluminescence spectra was measured to study the electron-hole pair recombination rate in the photocatalytic materials by utilizing an Agilent Technologies Cary Eclipse fluorescence spectrophotometer. The time-dependent absorption spectra were recorded on a Shimadzu UV-2450 spectrophotometer, in the wavelength range 200 nm to 800 nm. The Brunauer-Emmett-Teller (BET) surface area studies were carried out at 77 K on Quantachrome Autosorb-iQ-MP-XR system.

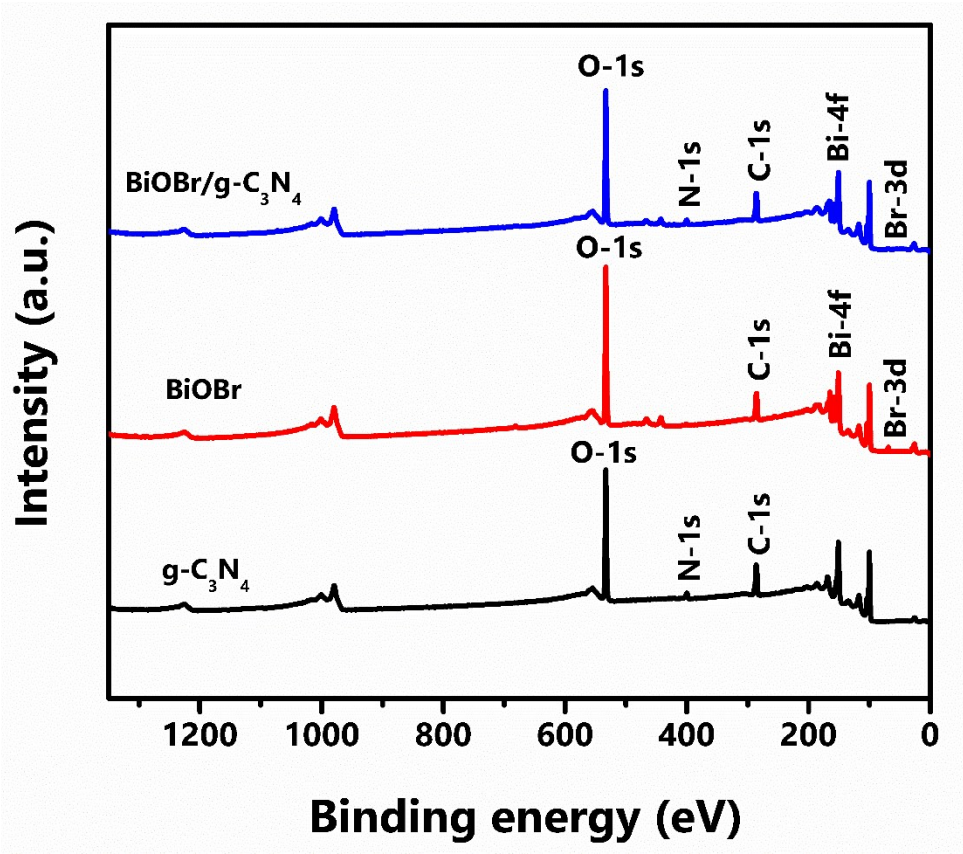

Fig. S1 XPS survey spectra of g-C_3N_4, BiOBr and BiOBr/g-C_3N_4 composite.

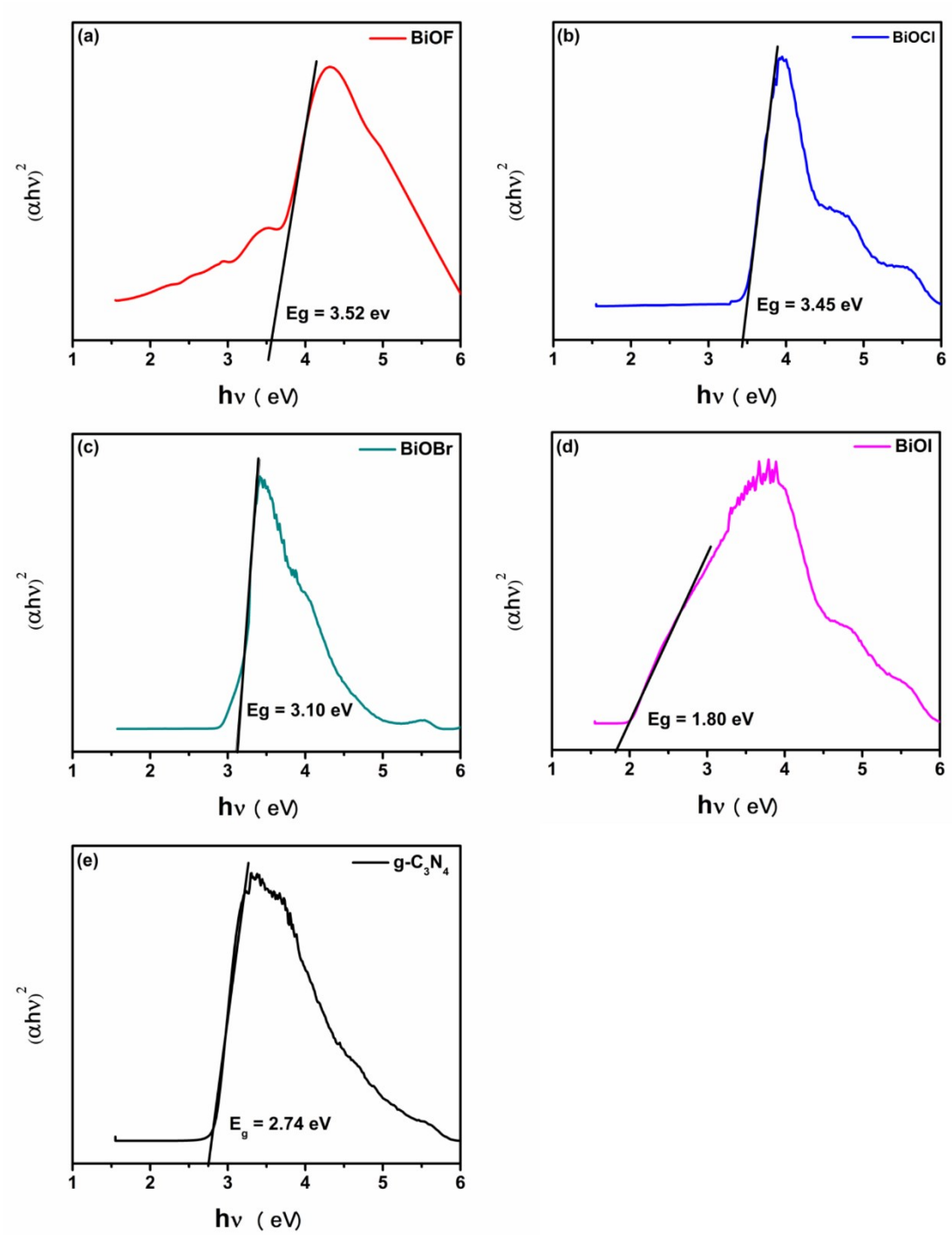

Fig. S2 Plot of transformed Kubelka–Munk function vs energy (Tauc plots): (a-d) for BiOX (X = F, Cl, Br and I) and (e) g-C_3N_4.

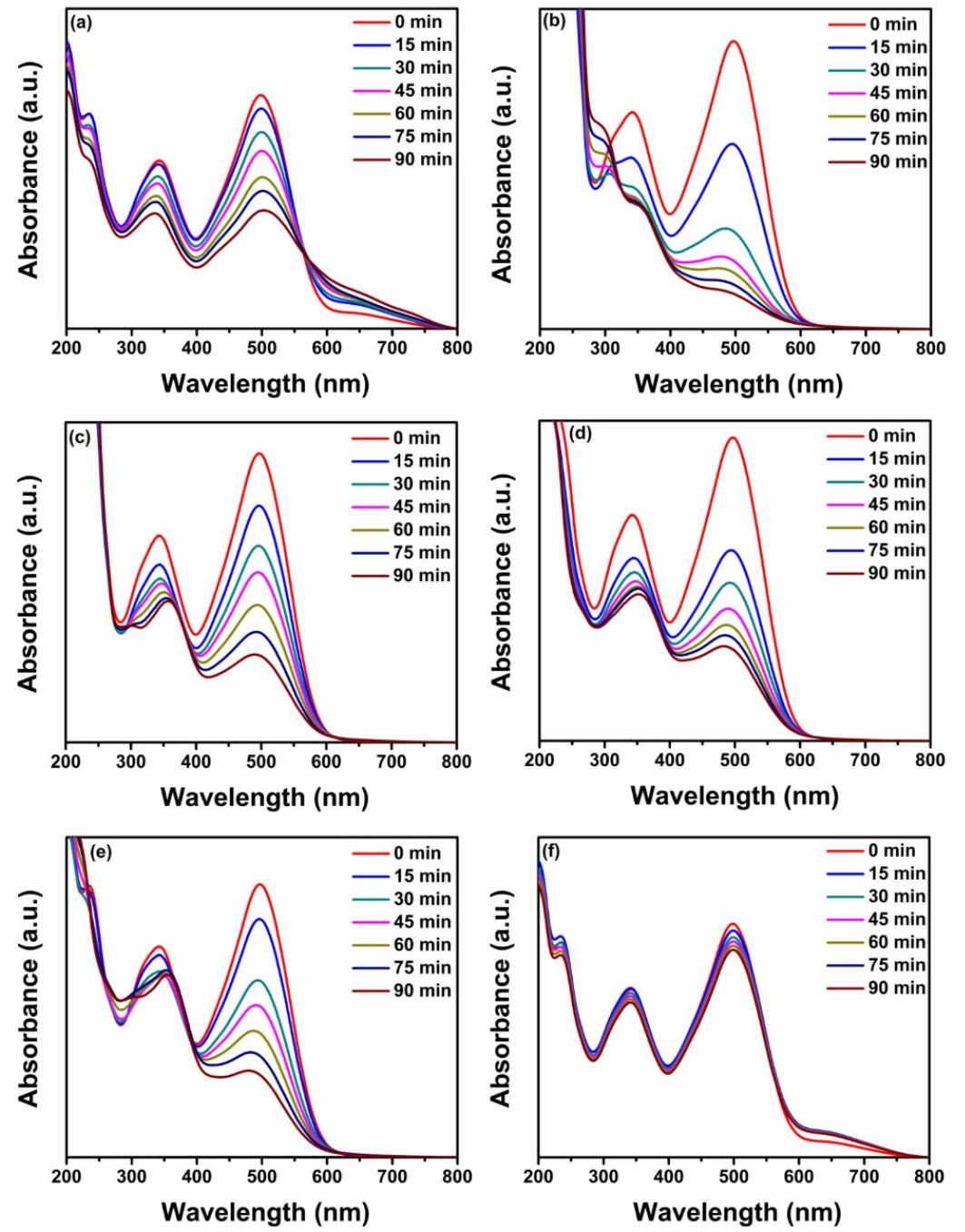

Fig. S3 Time dependent UV-vis absorption spectra of CR degradation using (a) BiOF, (b) BiOCl, (c) BiOBr, (d) BiOI, (e) g-C_3N_4 and (f) without any photocatalyst (photolysis).

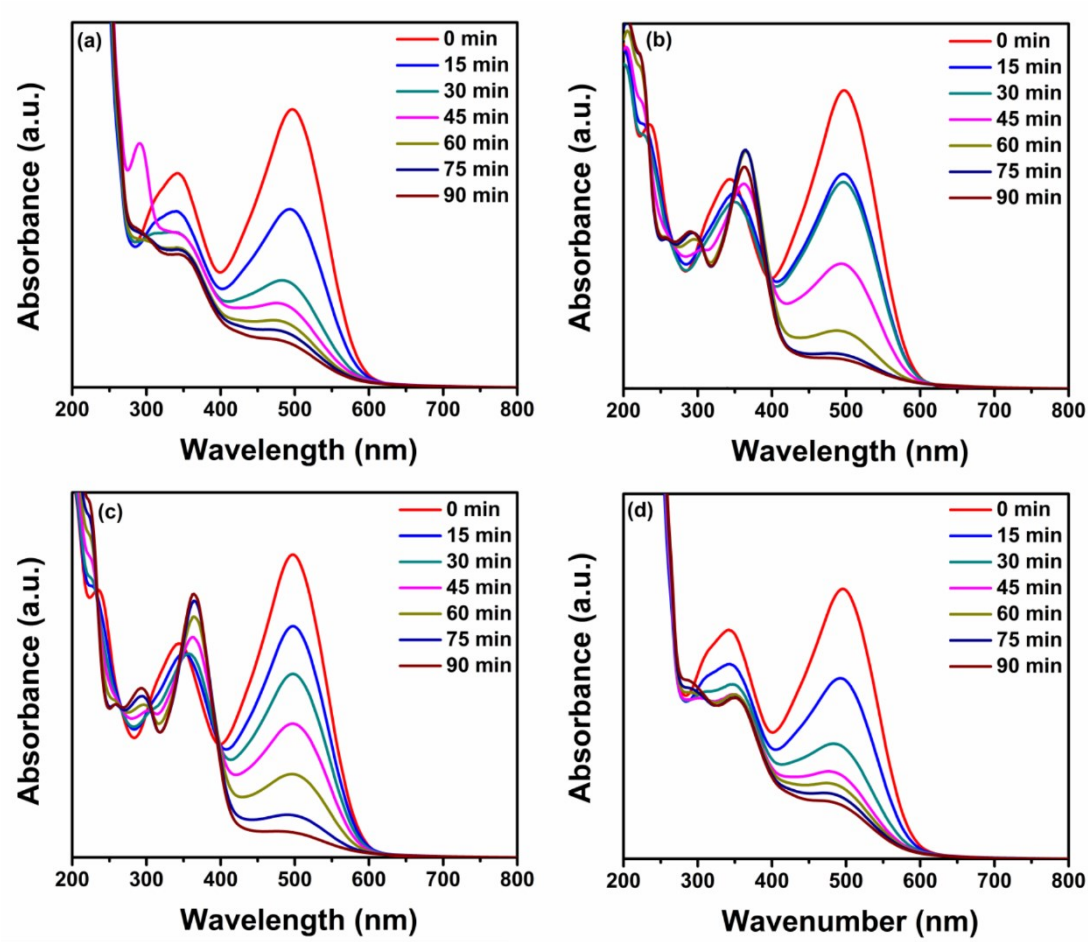

Fig. S4 Time dependent UV-vis absorption spectra of CR dye degradation using (a) BiOF/g-C_3N_4, (b) BiOCl/g-C_3N_4, (c) BiOBr/g-C_3N_4 and (d) BiOI/g-C_3N_4 composites.

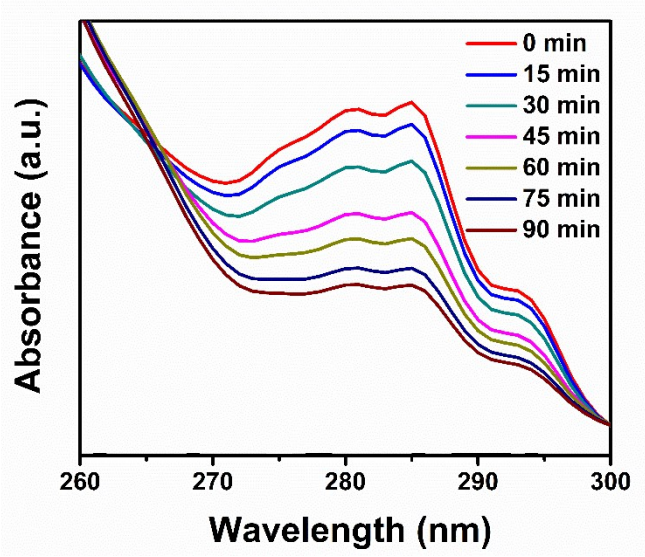

Fig. S5 Time dependent UV-vis absorption spectra of CBZ fungicide using BiOBr/g-C_3N_4 composite.

Table S1 Kinetics parameters for CR dye degradation over different photocatalysts.

Photocatalyst	**Rate constant k (min^{-1})**	**R^2 value**	**Half-life time $t_{1/2}$ (min)**
g-C_3N_4	0.013	0.993	53.308
BiOF	0.008	0.984	86.625
BiOCl	0.023	0.964	30.130
BiOBr	0.013	0.996	53.308
BiOI	0.012	0.952	57.750
BiOF/g-C_3N_4	0.020	0.957	35.000
BiOCl/g-C_3N_4	0.027	0.977	25.955
BiOBr/g-C_3N_4	0.028	0.957	25.109
BiOI/g-C_3N_4	0.018	0.963	39.152

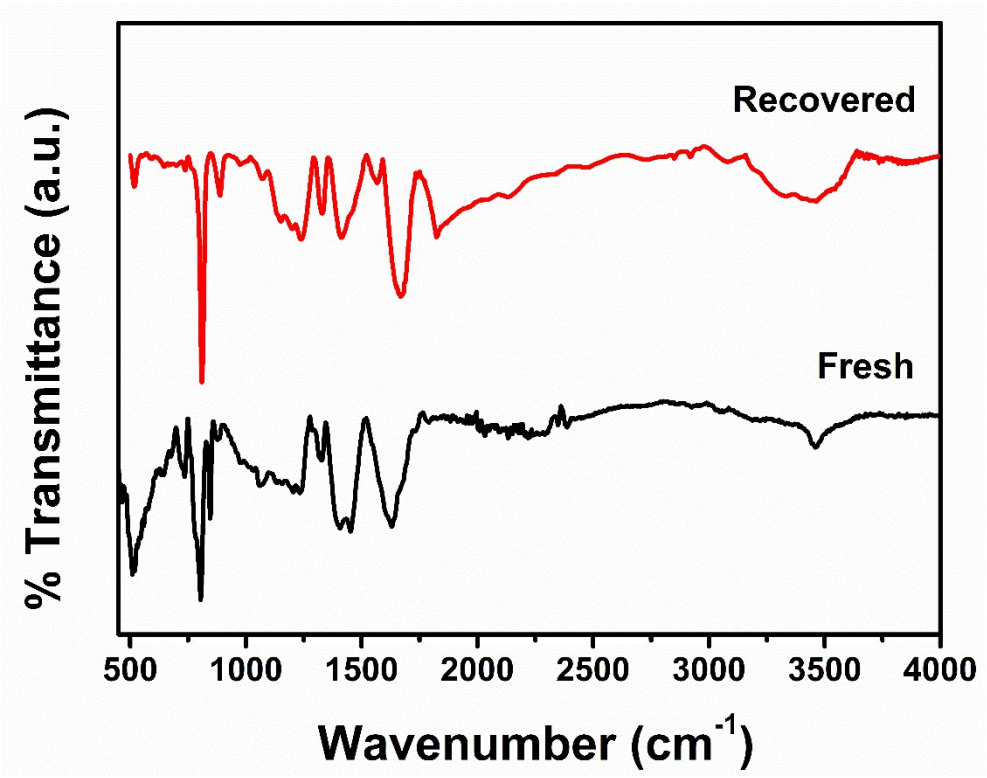

Fig. S6 FTIR spectra of fresh and recovered BiOBr/g-C_3N_4 composite.